05,12

Features of obtaining by the method of matrix synthesis, structure and magnetic properties of iron nanowires

© D.L. Zagorskiy[1], I.M. Doludenko[1], K.V. Frolov[1], I.V. Perunov[1], M.A. Chuev[2], N.K. Chumakov[3], I.V. Kalachikova[1], V.V. Artemov[1], T.V. Tziganova[1], S.S. Kruglikov[4]

[1] Institute of Crystallography of the Federal Scientific Research Center,
„Crystallography and Photonics“ Scientific Research Cener of the Russian Academy of Science„Kurchatov Institute“,
Moscow, Russia
[2] Valiev Institute of Physics and Technology, Russian Academy of Sciences,
Moscow, Russia
[3] National Research Center „Kurchatov Institute“,
Moscow, Russia
[4] Russian University of Chemistry and Technology named after D.I. Mendeleev
Moscow, Russia

E-mail: dzagorskiy@gmail.com

Received April 17, 2023
Revised April 17, 2023
Accepted May 11, 2023

Nanowires from iron were investigated. Samples in the form of arrays of parallel threads (wires) were obtained by matrix synthesis using track membranes. Matrices with parallel pores of 100 nm were used, and the growth voltage was varied — 0.8 V, 1 V and 1.2 V. Electron microscopic studies of the growth matrix and samples were carried out. The obtained data of Mössbauer spectroscopy and magnetometry correlate well. Thus, a comparison of the results obtained by these methods showed that with an increase in the deposition potential during the synthesis of nanowires, the misorientation angle of the magnetic moments of domains increases. It is also shown that as the deposition potential increases, the coercive force decreases.

Keywords: magnetic nanowires, matrix synthesis, structure, Mössbauer spectroscopy, magnetic properties.

DOI: 10.21883/PSS.2023.06.56104.11H

1. Introduction

Over the last 15 years, much research attention has focused on magnetic nanomaterials and nanostructures with strong shape anisotropy: nanowires (NW), strips, disks, curved surfaces, spirals [1–7], having potential applications in nanosensors, spintronic devices, quantum computer elements, biology and medicine. A significant number of results have been obtained for various types of magnetic NW, including rather complex compositions and/or shapes: from alloys based on 3d transition metals (Cr, Mn, Fe, Co, Ni, Cu), layered, hollow, profiled [8].

At the same time, there is still interest in the simplest types of NW — homogeneous, from a single metal, primarily because for them, it is possible to most accurately and correctly study and theoretically describe the influence of changing geometry and production conditions on the magnetic properties. The most common method of producing such NWs is matrix synthesis — filling narrow channels in a porous matrix with the desired material. Such a process is usually carried out electrochemically [9–11].

Many studies have studied iron NWs with diameters ranging from 5 to 500 nm, obtained in different matrices [12–22]. It has been shown that growth conditions strongly influence the crystallinity of NWs and their physical properties, in particular, their magnetic properties. It was found that among several major factors: electrolyte composition, matrix pore diameter and growth voltage, — the latter plays a significant role. In the study of magnetic properties, one of the most interesting effects from a practical point of view is the formation of spontaneous magnetization of NWs along their axis and high values of magnetic parameters — coercive force and residual magnetization.

However, a full understanding and correct theoretical description of these effects is difficult due to the significant variation in the parameters of the NWs themselves, synthesized under different conditions. In addition, commercial track membranes have usually been used as a polymer matrix, in which the pore axes, and hence the resulting NWs, have a dispersion of inclinations to the matrix plane, which has generally not been accounted for in theoretical models.

We have previously demonstrated the efficiency of theoretical description of the experimental results of magnetometry and Mössbauer spectroscopy on ^{57}Fe cores of iron-based NW arrays electrodeposited in the track pores of the polymer matrix using a generalized Stoner–Wolfart model [22–26]. This paper, within this approach, represents the results of a study of iron NW arrays electrodeposited at growth voltages of 0.8, 1.0 and 1.2 V into pores of a special

polymeric matrix, in which the pore axes are parallel to each other and perpendicular to the matrix surface.

2. Experiment procedure

Materials and instruments

Matrix. Polyethylene terephthalate track membranes $(C_{10}H_8O_4)_n$, manufactured at JINR, Dubna) were used as a growth matrix. The membranes had the following parameters: pore diameter — 100 nm; film thickness — 12 μm; pore density $\approx 1 \cdot 10^8$ cm^{-2}. The initial polymer film was irradiated with a beam of ions strictly perpendicular to the surface to form tracks parallel to each other and perpendicular to the surface of the matrix (film).

One side of the membrane was coated with a solid copper layer, which was used as a cathode. First, a thin layer of amorphous copper was formed by thermal spraying in a vacuum (VUP-4 unit), which was then thickened to 5–30 μm by electroplating. Subsequent electrodeposition of iron into the pores was carried out through the opposite surface of the matrix. The following electrolyte composition was used: $FeSO_4 \bullet 7H_2O$ — 120 g/l; H_3BO_3 — 25 g/l; sodium lauryl sulfate — 1 g/l (to increase matrix pore wetting). Ascorbic acid at a concentration of 1 g/l was used during deposition to prevent the transition of divalent Fe^{2+} iron ions to trivalent Fe^{3+}.

Electrodeposition. The electrodeposition took place in a galvanic cell. The potentiostat used as a source was an Elins P-2X galvanostat. The process was carried out in a two-electrode scheme, using an iron anode, at a deposition potential of $U = 0.8$ V, 1.0 and 1.2 V.

Electron microscopy and elemental analysis. Scanning electron microscopy (SEM) was performed with a JEOL JSM 6000 plus electron microscope equipped with an energy-dispersive elemental analysis attachment, at an accelerating voltage of 15 kV, in the secondary electron mode.

Magnetic measurements. The magnetization curves of all samples were measured at room temperature on a standard LakeShore 7407 vibrating magnetometer at 82 Hz. Each sample with a surface area of about 0.5 cm ^{2} was mounted on a flat holder and the external magnetic field $\boldsymbol{H}$ was directed perpendicular, at angles 45, 60° and parallel to the plane of the polymer membrane of the sample, which corresponded to the following set of mutual orientations of magnetic field and NW $\boldsymbol{L}$ axes in the membrane: $\varphi = 0°$ ($\boldsymbol{H} \parallel \boldsymbol{L}$), $\varphi = 45°$, $\varphi = 60°$ and $\varphi = 90°$ ($\boldsymbol{H} \perp \boldsymbol{L}$), accordingly. The magnitude of the magnetic field $\boldsymbol{H}$ varied cyclically between -5 and 5 kOe.

Mössbauer measurements. The Mössbauer transmission spectra of ^{57}Fe were measured at room temperature on a standard spectrometer MS-1104Em in constant acceleration mode with the gamma-ray source ^{57}Co(Rh) Ritverc MCo7.114 [27]. Isomeric shifts were calculated relative to a standard Ritverc MRA.2.6 absorber of α-Fe foil thickness 30 μm [28]. The collimated gamma ray flux was directed perpendicular to the plane of the polymer matrix so that the gamma ray wave vector $\boldsymbol{k}_\gamma$ coincides in direction with the axis $\boldsymbol{L}$ of the track pores and NWs $\boldsymbol{k}_\gamma \parallel \mathbf{L}$. Computer processing of the experimental spectra was performed using the Univem MS software included with the MS-1104Em spectrometer and DISCVER software [29–30].

Polymer matrix separation. Magnetic and Mössbauer measurements were carried out on NW arrays in a polymer matrix. For SEM, the polymer matrix was separated by the standard method of dissolving in concentrated alkali when heated to $T = 65$°C. To prevent oxidation of the iron NWs after removal of the polymer matrix, the array of isolated NWs was immediately placed in an electron microscope vacuum chamber.

3. Results and discussion

Matrix attestation. In a preliminary stage, the growth membrane was validated. The matrix cross section was made using the focused ion beam (FIB) method on a Scios DualBeam FEI electron microscope, the SEM image of which is shown in Fig. 1.

This image makes it possible to estimate the pore diameter, to confirm the mutual parallelism of the pore channels and their perpendicularity to the membrane surface.

Electrodeposition control. In order to control the galvanic process of iron deposition into the matrix pores at different potentials, chronoamperograms $I(t)$ were recorded and then analyzed as shown in Fig. 2, *a*.

The analysis of the resulting $I(t)$ dependences made it possible to determine the optimum deposition time, at which the growing NW material filled the track pore as much as possible, but did not exceed its limits (control — shown by arrows).

SEM results. Fig. 2, *b* shows an example of SEM-derived microphotographs. The NW diameter corresponded to the pore diameter of the matrix, and the growth rate

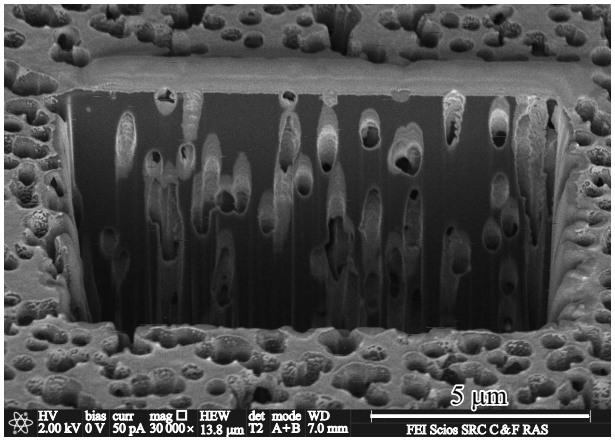

Figure 1. SEM image of a slightly inclined cross section of a polymer membrane made with a focused ion beam (FIB).

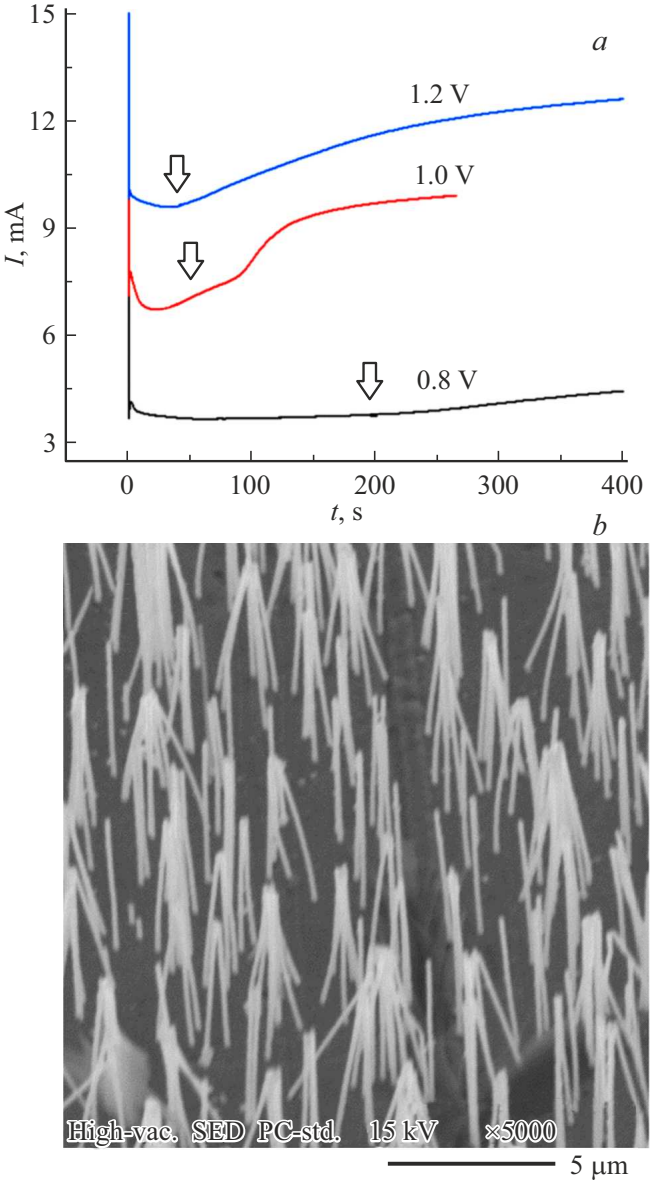

Figure 2. *a* — Chronoamperograms of electrodeposition $I(t)$ of iron NW test samples at different potentials, (arrows indicate deposition time for control samples);*b* — SEM image of the obtained iron NW samples after separation of the growth polymer matrix.

was estimated from the measured length of the NWs. Elemental analysis showed that the NWs obtained are entirely composed of iron. Fig. 2, *b* shows that some of the NWs stick together during the drying. Some NWs, however, are noticeably shorter than the average length in the array. We suggest that on the one hand, this could be due to the stopping of the NW growth in the channel of the corresponding pores due to its overlapping by the emitted hydrogen gas, and on the other hand — breaking off of individual NWs during removal of the polymer matrix and manipulation of the sample during transfer into the electron microscope chamber.

Table 1. Mössbauer hyperfine parameters for studied samples of NW arrays. δ — isomer shift, B_{hf} — hyperfine magnetic field on ^{57}Fe nuclei, $A_{2,5}$ — relative intensity 2 and 5 lines in magnetic sextet, $\Delta\Theta_{\text{ms}}$ — half angle of cone solution, within which the orientation of the magnetic moments of the domains within the NWs is distributed, calculated from Mössbauer measurements, G — the width of the Gaussian distribution of the hyperfine magnetic fields.

№	δ, mm/s	B_{hf}, T	$A_{2,5}$	$\Delta\Theta_{\text{ms}}$, °	G, T
0.8 V	0.018(9)	33.00(3)	0.436	38.0(1)	0.26(7)
1.0 V	−0.026(4)	33.05(2)	0.703	48.5(1)	0.40(3)
1.2 V	0.013(2)	32.92(1)	0.539	42.3(1)	0.30(2)

Since the directions of the hyperfine magnetic field on the ^{57}Fe $\boldsymbol{B}_{\text{hf}}$ nuclei and the magnetic moment of the spherical domain $\boldsymbol{M}$ coincide, in our case, the angle θ_{k} characterizes the deflection $\boldsymbol{M}$ from the NW $\boldsymbol{L}$ axis. If the orientation of moments $\boldsymbol{M}$ is strictly parallel to vector $\boldsymbol{k}_\gamma$ angle $\theta_{\text{k}} = 0$ and magnitude $A_{2,5} = 0$, and when the vectors $\boldsymbol{M}$ and $\boldsymbol{k}_\gamma$ are perpendicular angle $\theta_k = \pi/2$ and magnitude $A_{2,5} = 4$.

It has been shown earlier that the magnetic moments of single-domain spherical particles smaller than 20 nm in diameter in linear chains must be antiferromagnetic-ordered along the chains (one-dimensional antiferromagnetic ordering) [32], and Mössbauer spectra measured on arrays of magnetic NWs with diameters smaller than 20 nm show almost complete disappearance of line 2 and 5 in sexteth [33,34]. As the NW diameter increases, the single-domain state in the wire cross section is disturbed, resulting in a deviation in orientation of „light“ axes of magnetic domains within the NW from the direction of vector $\boldsymbol{k}_\gamma$ and the distribution of the hyperfine interaction parameters in the Mössbauer spectrum, which is determined by the average $\langle\cos^2\theta_{\text{k}}\rangle$ [35].

Deviation from the vector direction $\boldsymbol{k}_\gamma$ orientation of the NWs themselves, due to the mutual non-parallelism of the track pores in the standard polymer matrix, leads to an additional contribution to the distribution of the Mössbauer parameters. In order to remove (avoid) this contribution and to take into account (calculate) as correctly as possible the misorientation of the „light“ axes of the magnetic domains inside the NW, a specially prepared polymer matrix with track pores parallel to each other and perpendicular to its surface was used in this paper (see Fig. 1).

Mössbauer spectroscopy. The spectra of all samples show a characteristic six-linear magnetic splitting (Fig. 3, *a*) and are well approximated by a single sextet with hyperfine parameters corresponding to metallic α-Fe (see Table 2). The relative intensities of 2nd and 5th sextet lines significantly differ from the ratio $I_{1,6} : I_{2,5} : I_{3,4} = 3 : 2 : 1$ typical of polycrystalline materials, indicating the presence of spontaneous magnetization along the NW axes. It is known that in the magnetic hyperfine structure of the Mössbauer spectrum, the intensities of the sextet lines

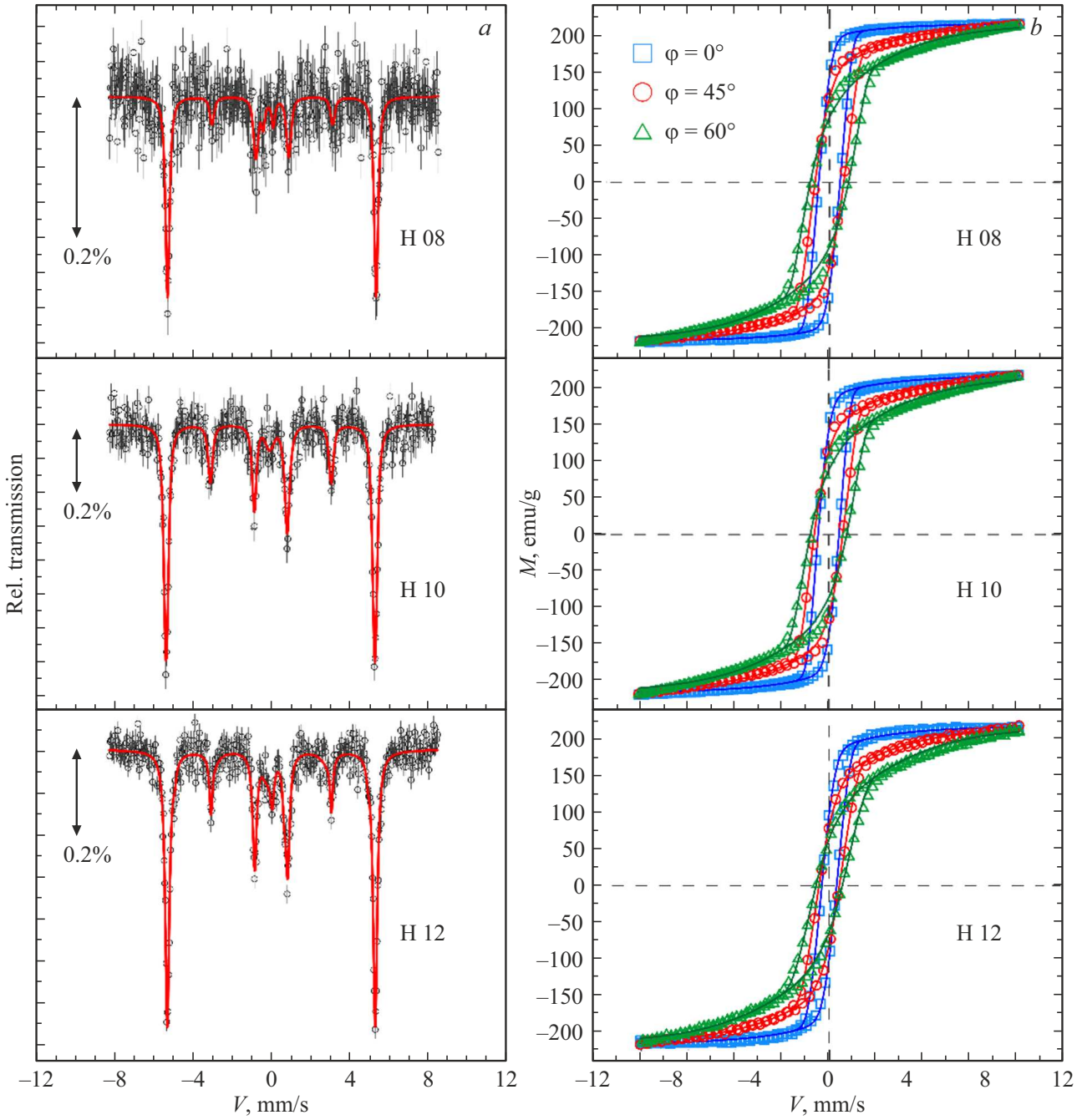

Figure 3. Mössbauer spectra (a) and magnetization curves (b) for H 08, H 10, H 12 iron NW arrays deposited at 0.8 V, 1.0 V and 1.2 V potentials, respectively.

satisfy the relations

$$I_{1,6} : I_{3,4} = 3 \quad \text{and} \quad I_{2,5} = A_{2,5} = 4\sin^2\theta/(1+\cos^2\theta_k),$$

where θ_k — the angle between the wave vector $\boldsymbol{k}_\gamma$ and the magnetic field direction $\boldsymbol{B}_{\mathbf{hf}}$ [31].

In Fig. 3, b — experimental points for different orientations of NW axes $\boldsymbol{L}$ in the array to the direction of external magnetic field $\boldsymbol{H}$ are shown: for the angle $\varphi = 0°$ — blue squares, $\varphi = 45°$ — red circles, $\varphi = 60°$ — green triangles. The continuous lines of the respective colors are drawn according to the results of a computational approximation performed within the generalized Stoner–Wolfart model.

Earlier in paper [22], we showed that the directions of magnetic moments of NW domains are distributed around the direction $\theta_k = 0$ in the interval $\Delta\Theta$ $(0 < \Delta\Theta < \pi/2)$ along the polar angle, i.e., in the cone of directions with the solution angle $2\Delta\Theta$ relative to the NW axes normal to the membrane surface. The values of the hyperfine parameters and angles calculated in the analysis of the Mössbauer spectra within this approach are shown in Table 1.

Table 2. Parameters of the magnetization curves for the studied samples of NW arrays. M_0 — saturation magnetization, K — magnetic anisotropy constant, D — effective average NW magnetic domain diameter, $\Delta D/D$ — comparative Gaussian width of domain diameter distribution, $\Delta\Theta_{mgn}$ — half cone solution angle, within which the orientation of the magnetic moments of the domains within the NW is distributed, calculated from magnetometry data, H_C — coercive force KV/k_BT — magnetic anisotropy energy, V — average volume of the magnetic domain

№	M_0, A · cm^2/kg	$K \cdot 10^{-7}$, J /m^3	D_{mgn}, nm	$\Delta D/D$	$\Delta\Theta_{mgn}$,	H_C, Oe	KV/k_BT
0.8 V	217.9(1)	1.74(1)	7.9(1)	0.13(1)	36.1(2)	450(10)	11.03(5)
1.0 V	218.1(1)	1.77(1)	7.9(1)	0.12(1)	45.1(4)	435(10)	11.21(4)
1.2 V	218.8(2)	1.76(1)	7.6(1)	0.13(1)	47.9(4)	330(10)	9.69(5)

Magnetic measurements. The measured magnetization curves are shown in Fig. 3, *b*. For all samples of NW arrays, the hysteresis loops exhibit the characteristic shape of ferromagnetics. Table 2 shows the experimental values of magnetic parameters at room temperature as well as calculated values of magnetic anisotropy constant K, magnetic anisotropy energy KV/kB, saturation magnetization M_0, critical magnetic field of domain remagnetization $H_C = 2K/M_0$, effective mean domain diameter D_0, relative width of Gaussian domain diameter distribution $\Delta D/D_0$. The calculated parameter values were obtained within the generalized Stoner–Wolfart model [36–38], already successfully used by us earlier in paper [26]. The approximation of the experimental magnetization curves (in Fig. 3, *b* shown by solid lines) for the values of the angle between the NW axis direction and the magnetic field $\boldsymbol{H}$ $\varphi > 45^\circ$ was unsatisfactory (see green approximation curve for $\varphi = 60^\circ$ in Fig. 3, *b*), which is due to the difficulty of (correct) accounting for the inhomogeneous magnetic field on a sample with a given geometric shape and dimensions.

It should be noted that the magnetization scatter angles $\Delta\Theta_{ms}$ and $\Delta\Theta_{mgn}$ obtained by the two methods (see Tables 1 and 2) are almost identical.

4. Conclusion

The modes to obtain iron NW array under different conditions were determined. SEM measurements confirmed the parallel alignment of the pores in the polymer matrix and the NWs grown therein, as well as their perpendicularity to the matrix surface.

The analysis of Mösbauer spectroscopy and magnetic measurements showed that:

– with increasing growth voltage most of the magnetic and Mössbauer parameters are virtually unchanged. At the same time, the distribution angle $2\Delta\Theta$ (the angle of the cone solution, within which the NW magnetization directions „were distributed“) increases and the coercive force of NW markedly decreases.

– the angle $2\Delta\Theta$ of the magnetization direction distribution of arrays „parallel“ to NWs with a diameter of 100 nm is quite large, which is obviously due to the small size of magnetic domains, whose packing inside the NW is far from quasi-dimensional chains of spheres. It follows from the obtained $2\Delta\Theta$ values for arrays „parallel“ NWs that the contribution to the NW axis tilt distribution in conventional polymeric track membranes is not very large and is no more than $10-15^\circ$.

– magnetic measurements at different orientations of the sample relative to the direction of the external magnetic field and calculated values of the magnetic anisotropy energy KV/k_BT demonstrated a strong anisotropy of the magnetic properties and high resistance of the NW to remagnetization (demagnetization).

Thus, it is shown that changing the growth potential of the deposition can be used to control the magnetic parameters of the NW.

Acknowledgments

This paper was supported by the Russian Science Foundation grant 22-22-00983.

Conflict of interest

The authors declare that they have no conflict of interest.

References

[1] J. Ping Liu, E. Fullerton, O. Gutfleisch, D.J. Sellmyer. Nanoscale Magnetic Materials and Applications. Springer Dordrecht, Heidelberg, London, N.Y. (2009). 732 p.
[2] D.Y. Nam, S.H. Kim, Y.S. Jeon, Y.K. Kim. IEEE Transact. Magn. **53**, *11*, 1 (2017).
[3] D.Y. Nam, A.Y. Samardak, Y.S. Jeon, S.H. Kim, A.V. Davydenko, A.V. Ognev, A.S. Samardak. Y.K. Kim. Nanoscale **10**, 20405 (2018).
[4] R. Streubel, P. Fischer, F. Kronast, V.P. Kravchuk, D.D. Sheka, Y. Gaididei, O.G. Schmidt, D. Makarov. Phys. D **49**, 363001 (2016).
[5] D. Gregurec, A.W. Senko, A. Chuvilin, P.D. Reddy, A. Sankararaman, D. Rosenfeld, P.H. Chiang, F. Garcia, I. Tafel, G. Varnavides, E. Ciocan, P. Anikeeva. ACS Nano **14**, *7*, 8036 (2020).
[6] T.N. Zamay, V.S. Prokopenko, S.S. Zamay, K.A. Lukyanenko, O.S. Kolovskaya, V.A. Orlov, G.S. Zamay, R.G. Galeev, A.A. Narodov, A.S. Kichkailo. Nanomaterials **11**, *6*, 1459 (2021).

[7] J. Xia, X. Zhang, X. Liu, Y. Zhou, M. Ezawa. Commun. Mater. **3**, 88 (2022).
[8] M. Vazquez. Magnetic Nano- and Microwires. Design, Synthesis. Properties and Applications. Woodhead Publishing (2020). 997 p.
[9] C.R. Martin. Science **266**, *23*, 1961 (1994).
[10] S.K. Chakarvarti, J. Vetter. Nucl. Instr. Meth. Phys. Res. B **62**, *1*, 109 (1991).
[11] J. Vetter, R. Spohr. Nucl. Instrum. Meth. Phys. Res. B **79**, *1–4*, 691 (1993).
[12] D. Dobrev, J. Vetter, N. Angert, R. Neumann. Appl. Phys. A **72**, 729 (2001).
[13] D. Borissov, S. Isik-Uppenkamp, M. Rohwerder. J. Phys. Chem. C **113**, *8*, 3133 (2009).
[14] X.Y. Zhang, G.H. Wen, Y.F. Chan, R.K. Zheng, X.X. Zhang, N. Wang. Appl. Phys. Lett. **83**, *16*, 3341 (2003).
[15] Y.L. Sun, Y. Dai, L.Q. Zhou, W. Chen. Solid State Phenom. **121–123**, *3*, 17 (2007).
[16] J. Verbeeck, O.I. Lebedev, G.V. Tendeloo, L. Cagnon, C. Bougerol, G. Tourillon. J. Electrochem. Soc. **150**, *10*, 468 (2003).
[17] G. Tourillon, L. Pontonnier, J.P. Levy, V. Langlais. Electrochem. Solid State Lett. **3**, *1*, 20 (2000).
[18] J.M. Baik, M. Schierhorn, M. Moskovits. J. Phys. Chem. C **112**, *7*, 2252 (2008).
[19] V. Haehnel, S. Fähler, P. Schaaf, M. Miglierini, C. Mickel, L. Schultz, H. Schlörb. Acta Mater. **58**, *7*, 2330 (2010).
[20] Y. Peng, H.L. Zhang, S.L. Pan, H.L. Lia J. Appl. Phys. **87**, *10*, 7405 (2000).
[21] L. Menon, M. Zheng, H. Zeng, S. Bandyopadhyay, D.J. Sellmyer. J. Electron. Mater. **29**, *5*, 510 (2000).
[22] K.V. Frolov, D.L. Zagorsky, I.S. Lyubutin, M.A. Chuev, I.V. Perunov, S.A. Bedin, A.A. Lomov, V.V. Artemov, S.N. Sulyanov. Pis'ma v ZhETF **105**, *5*, 297 (2017). (in Russian).
[23] K.V. Frolov, D.L. Zagorsky, I.S. Lyubutin, V.V. Korotkov, S.A. Bedin, S.N. Sulyanov, V.V. Artemov, B.V. Mchedlishvili. Pis'ma v ZhETF **99**, *10*, 656 (2014). (in Russian).
[24] D.L. Zagorsky, K.V. Frolov, S.A. Bedin, I.V. Perunov, M.A. Chuev, A.A. Lomov, I.M. Doludenko. FTT **60**, *11*, 2075 (2018). (in Russian).
[25] I.M. Doludenko, D.L. Zagorsky, K.V. Frolov, I.V. Perunov, M.A. Chuev, V.M. Kanevsky, H.C. Yerokhina, S.A. Bedin. FTT **62**, *9*, 1474 (2020). (in Russian).
[26] K.V. Frolov, M.A. Chuev, I.S. Lyubutin, D.L. Zagorskii, S.A. Bedin, I.V. Perunov, A.A. Lomov, V.V. Artemov, D.N. Khmelenin, S.N. Sulyanov, I.M. Doludenko. J. Magn. Magn. Mater. **489**, 165415 (2019).
[27] https://ritverc.com/en/products/sources-scientific-application/mossbauer-sources/57co
[28] https://ritverc.com/en/products/sources-scientific-application/mossbauer-sources/reference-absorbers
[29] M.A. Chuev. Dokl. Phys. **56**, 318 (2011).
[30] M.A. Chuev, V.M. Cherepanov, M.A. Polikarpov. JETP Lett. **92**, *1*, 21 (2010).
[31] P. Gütlich, E. Bill, A.X. Trautwein. Mössbauer Spectroscopy and Transition Metal Chemistry: Fundamentals and Applications. Springer Verlag, Berlin, Heidelberg (2011). 568 p.
[32] I.S. Jacobs, C.P. Bean. Phys. Rev. **100**, 1060 (1955).
[33] Y. Peng, H.L. Zhang, S.L. Pan, H.L. Li. J. Appl. Phys. **87**, *10*, 7405 (2000).
[34] Z. Chen, Q. Zhan, D. Xue, F. Li, X. Zhou, H. Kunkel, G. Williams. J. Phys. Condens. Matter **14**, *3*, 613 (2002).
[35] M.A. Chuev, V.M. Cherepanov, M.A. Polikarpov. JETP Lett. **92**, *1*, 21 (2010).
[36] E.C. Stoner, E.P. Wohlfarth. Philos. Trans. R. Soc. A **240**, 599 (1948).
[37] A.M. Afanas'ev, M.A. Chuev, J. Hesse. Exp. Theor. Phys. **89**, 533 (1999).
[38] M.A. Chuev, J. Hesse. J. Phys. Condens. Matter **19**, 506201 (2007).

Translated by Ego Translating